

**Temperature-  
dependent  
accumulation mode  
particle**

L. Ahlm et al.

# Temperature-dependent accumulation mode particle and cloud nuclei concentrations from biogenic sources during WACS 2010

L. Ahlm<sup>1,\*</sup>, K. M. Shakya<sup>1</sup>, L. M. Russel<sup>1</sup>, J. C. Schroder<sup>2</sup>, J. P. S. Wong<sup>3</sup>,  
S. J. Sjostedt<sup>4,\*\*</sup>, K. L. Hayden<sup>4</sup>, J. Liggi<sup>4</sup>, J. J. B. Wentzell<sup>4</sup>, H. A. Wiebe<sup>4</sup>,  
C. Mihele<sup>4</sup>, W. R. Leitch<sup>4</sup>, and A. M. Macdonald<sup>4</sup>

<sup>1</sup>Scripps Institution of Oceanography, University of California, San Diego, La Jolla, California, USA

<sup>2</sup>Department of Chemistry, University of British Columbia, Vancouver, BC, Canada

<sup>3</sup>Department of Chemistry, University of Toronto, Toronto, Ontario, Canada

<sup>4</sup>Science and Technology Branch, Environment Canada, Toronto, Ontario, Canada

\* now at: Department of Applied Environmental Science, Stockholm University, Sweden

\*\* now at: Department of Chemistry and Biochemistry, Georgia Institute of Technology, Atlanta, Georgia, USA

Title Page

Abstract

Introduction

Conclusions

References

Tables

Figures

⏪

⏩

◀

▶

Back

Close

Full Screen / Esc

Printer-friendly Version

Interactive Discussion



Received: 12 October 2012 – Accepted: 17 October 2012 – Published: 24 October 2012

Correspondence to: L. M. Russell (lmrussell@ucsd.edu)

Published by Copernicus Publications on behalf of the European Geosciences Union.

Discussion Paper | Discussion Paper | Discussion Paper | Discussion Paper | Discussion Paper

ACPD

12, 27989–28031, 2012

---

**Temperature-  
dependent  
accumulation mode  
particle**

L. Ahlm et al.

---

Title Page

Abstract

Introduction

Conclusions

References

Tables

Figures



Back

Close

Full Screen / Esc

Printer-friendly Version

Interactive Discussion

27990



## Abstract

Submicron aerosol particles collected simultaneously at the mountain peak (2182 m a.s.l.) and at a forested mid-mountain site (1300 m a.s.l.) on Whistler Mountain, British Columbia, Canada, during June and July 2010 were analyzed by Fourier transform infrared (FTIR) spectroscopy for quantification of organic functional groups. Positive matrix factorization (PMF) was applied to the FTIR spectra. Three PMF factors associated with (1) combustion, (2) biogenics, and (3) vegetative detritus, were identified at both sites. The biogenic factor was correlated with both temperature and several volatile organic compounds (VOCs). The combustion factor dominated the submicron particle mass during the beginning of the campaign when the temperature was lower and advection was from the Vancouver area, but as the temperature started to rise in early July the biogenic factor came to dominate as a result of increased emissions of biogenic VOCs and thereby increased formation of secondary organic aerosol (SOA). On average, the biogenic factor represented 69 % and 49 % of the submicron organic particle mass at Whistler Peak and at the mid-mountain site, respectively. The lower fraction at the mid-mountain site was a result of more vegetative detritus there, and also higher influence from local combustion sources.

The biogenic factor was strongly correlated ( $r \sim 0.9$ ) to number concentration of particles with diameter ( $D_p$ ) > 100 nm, whereas the combustion factor was better correlated to number concentration of particles with  $D_p < 100$  nm ( $r \sim 0.4$ ). The number concentration of cloud condensation nuclei (CCN) was correlated ( $r \sim 0.7$ ) to the biogenic factor for supersaturations ( $S$ ) of 0.2 % or higher, which indicates that particle condensational growth from biogenic vapors was an important factor in controlling the CCN concentration for clouds where  $S \geq 0.2$  %. Both the number concentration of particles with  $D_p > 100$  nm and numbers of CCN for  $S \geq 0.2$  % were correlated to temperature. Considering the biogenic influence, these results indicate that temperature was a primary factor controlling these CCN concentrations at 0.2 % supersaturation.

### Temperature-dependent accumulation mode particle

L. Ahlm et al.

Title Page

Abstract

Introduction

Conclusions

References

Tables

Figures



Back

Close

Full Screen / Esc

Printer-friendly Version

Interactive Discussion



## 1 Introduction

Atmospheric aerosols affect climate by scattering and absorbing incoming solar radiation, and by acting as cloud condensation nuclei (CCN). The climatic impact of aerosol particles depends on their size and composition. Organic aerosols make up a significant fraction (20–90 %) of the sub-micrometer particulate mass (e.g. Jimenez et al., 2009). Whereas the formation process of inorganic aerosols such as sulfate, nitrate, and ammonium is fairly well understood, large uncertainties remain concerning the formation of secondary organic aerosol (SOA) from oxidation products of volatile organic compounds (VOCs) (e.g. Hallquist et al., 2009). Globally, emissions of biogenic VOCs (BVOCs) are estimated to be an order of magnitude larger than anthropogenic VOCs (Goldstein and Galbally, 2007), and oxidation of BVOCs yields a large biogenic contribution to SOA, estimated to be in the range 12–70 Tg yr<sup>-1</sup> (Hallquist et al., 2009). The SOA concentration has been predicted to increase by over 100 % until the year 2100 (Tsigaridis and Kanakidou, 2007) due to future expansion of boreal and temperate forests, and thereby increasing BVOC emissions.

The forested regions surrounding Whistler, BC, Canada, present a large source of biogenic aerosols and trace gases that have previously been the center for biogenic particle studies (Schwartz et al., 2010; Leaitch et al., 2011; Takahama et al., 2011). Schwartz et al. (2010) quantified organic aerosol functional groups at a mid-mountain site at Whistler Mountain in May and June 2008 using Fourier transform infrared (FTIR) spectroscopy. By applying positive matrix factorization (PMF) to FTIR spectra and investigating correlations between factors and tracers, they estimated that 65 % of the organic mass was from biogenic sources, and the remaining fraction from combustion sources. Takahama et al. (2011) performed similar measurements at Whistler Mountain in 2009, and in addition to biogenic and combustion aerosols also observed biomass burning particles. Leaitch et al. (2011) found an exponential increase in the submicron organic aerosol mass concentration with increasing temperature consistent with modeled emissions of BVOCs as a function of temperature.

### Temperature-dependent accumulation mode particle

L. Ahlm et al.

Title Page

Abstract

Introduction

Conclusions

References

Tables

Figures



Back

Close

Full Screen / Esc

Printer-friendly Version

Interactive Discussion



---

## Temperature-dependent accumulation mode particle

L. Ahlm et al.

---

Title Page

Abstract

Introduction

Conclusions

References

Tables

Figures

⏪

⏩

◀

▶

Back

Close

Full Screen / Esc

Printer-friendly Version

Interactive Discussion



The Whistler Aerosol and Cloud study (WACS) 2010, a large measurement campaign with focus on aerosols and clouds at Whistler Mountain, was carried out in June and July 2010. Macdonald et al. (2012) give an overview of the campaign, and found that organic compounds largely dominated the aerosol throughout most of the campaign. In this study, we focus on the organic aerosol during WACS 2010, and investigate the sources responsible for the organic aerosol mass during four periods with different meteorological conditions and advection from different areas. In addition, we investigate the sources or processes that control the particle number concentration. Finally we explore links between the organic aerosol and CCN concentrations, and the sources and processes that controlled the CCN population during this campaign. Unlike previous campaigns at Whistler, we use aerosol and gas-phase data sampled simultaneously at two different sites at different altitudes on Whistler Mountain, in order to investigate local sources, formation and transport of organic aerosols.

## 2 Sites and methods

### 2.1 Field sites

The measurements in this study were performed simultaneously at two sites on Whistler Mountain: Whistler Peak (WHI) at an altitude of 2182 m a.s.l.; and Raven's Nest (WRN), a mid-mountain site at 1300 m a.s.l. Raven's Nest is located near halfway between Whistler Village (650 m a.s.l.) and WHI.

WHI is approximately 400 m above the tree line. Raven's Nest is surrounded by forest composed mostly of coniferous trees like fir, hemlock and cedar trees. These sites may also be influenced from biomass burning aerosols in the summer, but during WACS 2010 such an influence was present only during the last three days of the study. Vancouver is the closest large city to Whistler, located approximately 100 km to the south. The two sites employed in this study are described more extensively in Macdonald et al. (2012), Pierce et al. (2012), and Wong et al. (2012).

## 2.2 Experimental

### 2.2.1 Filter sampling and analysis

Submicron particles were collected on 37 mm Teflon filters (Teflo, Pall Inc., Ann Arbor, MI) at both Raven's Nest and Whistler Peak. At Raven's Nest, the filters were sampled from 21 June to 28 July. All filters at Raven's Nest were sampled for 24 h, and were changed at 09:00 h local time (LT) every morning. The sampling setup included two filters sampled simultaneously, one with a diffusion dryer located upstream of the holder. In this manner dried and non-dried aerosol was sampled simultaneously.

At Whistler Peak, filters were sampled from 19 June to 28 July. The mean sampling times were three days for the period 19 June–2 July and 24 h from 2 July to 28 July. The filters were changed at 09:00 h LT. The sampler did not include a dryer at Whistler Peak. Filters were housed in a refrigerator at ca. 5 °C during sampling to reduce volatilization of organic compounds.

At both sites, a duplicate back filter was located behind each sampling filter to provide a measurement for adsorption during sampling and contamination during handling and storage. After sampling, the filters were kept frozen to prevent volatilization of the aerosol.

Fourier transform infrared (FTIR) spectroscopy was used to quantify organic functional groups of the aerosol samples, including alkane, alkene, hydroxyl, carboxylic acid, non-acidic carbonyl, primary amine, and organonitrate groups. Each filter was scanned both before and after sampling using a Bruker Tensor 27 FTIR Spectrometer with a deuterated tryglycine sulfate (DTGS) detector (Bruker, Waltham). The pre-scanned spectrum was subtracted from the post-scanned spectrum in order to correct for absorption by the Teflon filter itself. An algorithm described by Russell et al. (2009) was used to provide baselining, peak-fitting, and error estimation. The dried and non-dried filter samples from Raven's Nest had close to identical functional group concentrations resulting from the FTIR analysis. Therefore, throughout this paper only the non-dried filters from Raven's Nest will be included in the discussion, for a more direct

## Temperature-dependent accumulation mode particle

L. Ahlm et al.

Title Page

Abstract

Introduction

Conclusions

References

Tables

Figures



Back

Close

Full Screen / Esc

Printer-friendly Version

Interactive Discussion



comparison with those at Whistler Peak where no dryer was involved in the filter sampling.

Organosulfate groups were investigated by a method described by Russell et al. (2009), where filter samples are rinsed with hexane to separate organosulfate groups from bisulfate and carbonate since these compounds all have absorbance peaks at  $876\text{ cm}^{-1}$ . However, none of the filters had organosulfate concentrations above detection limit after rinsing.

Most of the filter samples, from both Whistler Peak and Raven's Nest, were also analyzed with X-ray fluorescence (XRF) which provides elemental composition of the aerosol, including all elements heavier than Na (Maria et al., 2003). The XRF analysis was conducted by Chester LabNet (Tigard, Oregon).

### 2.2.2 Spectromicroscopy

Particles were also collected on silicon nitride windows ( $\text{Si}_3\text{N}_4$ , Silson Ltd.), and were later analyzed by Scanning Transmission X-ray Microscopy with Near-Edge X-ray Absorption Fine Structure (STXM-NEXAFS) spectroscopy at the Advanced Light Source (ALS) at Lawrence Berkeley National Laboratories (Beamline 5.3.2). Particles were analyzed for carbon K-edge by scanning at energy levels between 278 and 320 eV (Kilcoyne et al., 2003). Spectra from ALS were processed using algorithms developed by Takahama et al. (2010), and using aXis software (Hitchcock, 2000). These measurements and the described analysis provide information of single particle organic functional groups of carbon containing particles as well as their size and morphology (Takahama et al., 2007).

### 2.2.3 Complementary measurements

The non-refractory chemical components of the submicron aerosol particles were measured using aerosol mass spectrometry at both Whistler Peak and Raven's Nest. An Aerodyne Compact Time-of-Flight Aerosol Mass Spectrometer (C-ToF-AMS)

## Temperature-dependent accumulation mode particle

L. Ahlm et al.

Title Page

Abstract

Introduction

Conclusions

References

Tables

Figures

⏪

⏩

◀

▶

Back

Close

Full Screen / Esc

Printer-friendly Version

Interactive Discussion



(Drewnick et al., 2005) was used at Whistler Peak, and a High-Resolution Time-of-Flight aerosol mass spectrometer (HR-ToF-AMS) (DeCarlo et al., 2006) was used at Raven's Nest.

Particle number size distributions were measured with TSI Scanning Mobility Particle Sizers (SMPS). An SMPS (3081L column and 3775 CPC) was used at Whistler Peak for particles in the 14–600 nm diameter interval, and at Raven's Nest for particles in the 16–700 nm diameter interval.

Number concentrations in the 0.65–20  $\mu\text{m}$  diameter interval were measured with a TSI Aerodynamic Particle Sizer (APS) at Raven's Nest. At Whistler Peak, number concentrations in the 0.25–32  $\mu\text{m}$  diameter interval were measured with an Optical Particle Counter (OPC).

Numbers concentrations of CCN at different supersaturations ( $S$ ), in the range 0.07–1.0 %, were measured with a CCN counter from Droplet Measurement Technologies, Inc. (DMT-200 CCN counter) (Roberts et al., 2003).

Black carbon (BC) number concentrations with a mass equivalent diameter interval of 90–270 nm were measured at each site with a Single Particle Soot Photometer (SP2), from Droplet Measurement Technologies, Inc.

Mixing ratios of several VOCs were measured using Proton Transfer Reaction Mass Spectrometry (PTR-MS). A quadrupole PTR-MS was used at Whistler Peak, and a time-of-flight PTR-MS (PTR-ToF-MS) was used at Raven's Nest.

Measurements of NO and NO<sub>2</sub> were conducted at both Whistler Peak and Raven's Nest using a chemiluminescence-based NO/NO<sub>x</sub> instrument (Thermo Scientific Model 42C-TL) with a photolytic converter specific for NO<sub>2</sub> detection. In addition, meteorological measurements of parameters including temperature, relative humidity, and wind speed were made at both sites.

---

## Temperature-dependent accumulation mode particle

L. Ahlm et al.

---

[Title Page](#)[Abstract](#)[Introduction](#)[Conclusions](#)[References](#)[Tables](#)[Figures](#)[⏪](#)[⏩](#)[◀](#)[▶](#)[Back](#)[Close](#)[Full Screen / Esc](#)[Printer-friendly Version](#)[Interactive Discussion](#)

### 3 Results and discussion

#### 3.1 Time series

Most measurements in this study were performed during the time period of the WACS 2010 campaign, 20 June to 28 July 2010. During this period organics contributed on average 89 % at Whistler Mountain and 74 % at Raven's Nest to the submicron particle mass sampled by the AMS. The corresponding contribution from sulfate was only 7 % and 19 %, respectively, at the two sites, and the contributions from ammonium and nitrate were below 5 % at both sites.

The WACS 2010 campaign is divided into four different periods based on differences in meteorology, air mass back trajectories, and aerosol and gas-phase chemistry (Macdonald et al., 2012). Period 1, covering the start of the campaign to 5 July, was characterized by cloudy conditions, low temperatures and snow remaining at both Whistler Peak and Raven's Nest. Back trajectories were predominantly from the south or southwest during this period (Fig. 1a), indicating advection from the Vancouver area. The average FTIR organic aerosol concentrations during period 1 were  $1.7 \mu\text{g m}^{-3}$  and  $1.0 \mu\text{g m}^{-3}$  at Raven's Nest and Whistler Peak, respectively. The organic aerosol was dominated by alkane and carboxylic acid groups at both sites (Fig. 2a–b), which is typical for an aerosol associated with anthropogenic combustion (e.g. Schwartz et al., 2010; Takahama et al., 2011). Few filters at Whistler Peak belonging to period 1 were analyzed by XRF, but from the XRF concentrations in the filters sampled at Raven's Nest (Fig. 2f) the concentrations of the submicron dust elements Al, Si, Ca, and Fe were relatively low during this period compared to the later periods. Also concentrations of coarse mode particle number concentrations were low during period 1 (Fig. 2g), indicating low dust concentrations for particles larger than  $1 \mu\text{m}$ .

Period 2 (5 July–11 July) was initiated by rapidly increasing temperature, which was followed by increased concentrations of monoterpene, isoprene, MVK/MACR (Fig. 2c–d), accompanied by increasing concentrations of organic aerosols (Fig. 2a–b). Organic aerosol concentrations, as quantified by the FTIR analysis, reached almost

## Temperature-dependent accumulation mode particle

L. Ahlm et al.

Title Page

Abstract

Introduction

Conclusions

References

Tables

Figures

⏪

⏩

◀

▶

Back

Close

Full Screen / Esc

Printer-friendly Version

Interactive Discussion



**Temperature-dependent accumulation mode particle**

L. Ahlm et al.

Title Page

Abstract

Introduction

Conclusions

References

Tables

Figures

⏪

⏩

◀

▶

Back

Close

Full Screen / Esc

Printer-friendly Version

Interactive Discussion

8  $\mu\text{g m}^{-3}$  at Raven's Nest, and 4  $\mu\text{g m}^{-3}$  at Whistler Peak on 10–11 July. The average FTIR organic concentrations during period 2 were 3.7 and 2.4  $\mu\text{g m}^{-3}$  at Raven's Nest and Whistler Peak, respectively. At Raven's Nest, the alcohol groups were at very high levels (Fig. 2b) reaching 3.1  $\mu\text{g m}^{-3}$  on 10 July. At Whistler Peak, the alcohol concentration reached a maximum of only 1.1  $\mu\text{g m}^{-3}$  during period 2. The alkane and carboxylic acid groups had rather similar concentrations at the two sites. Unlike period 1, period 2 had significant concentrations of non-acid carbonyl reaching a maximum of 1.2  $\mu\text{g m}^{-3}$  at Raven's Nest, and 0.7  $\mu\text{g m}^{-3}$  at Whistler Peak. Advection was during this period initially from the northerly areas changing to easterly later during the period (Fig. 1b). The areas to the north and east of Whistler have relatively few anthropogenic sources. The skies were mostly clear with occasionally a few scattered cumulus based several hundred meters above the Whistler Peak site. That observation together with strong diurnal variations in meteorological parameters such as temperature and relative humidity at Whistler Peak indicates that the mixed layer grew well above the peak of the mountain in daytime. The snow rapidly melted at Raven's Nest during period 2 and the warm and dry conditions contributed to higher concentrations of XRF dust elements (Fig. 2f) and coarse mode particles (Fig. 2g). Snow, however, remained at Whistler Peak where concentrations of dust were considerably lower (Fig. 2e), consistent with the observation of dust generated near Raven's Nest from mountain bikes and occasional vehicles.

Period 3, covering 12–22 July, was significantly warmer than period 1 but cooler than period 2. Concentrations of monoterpenes, isoprene, MVK, MACR, and organic aerosols were lower than during period 2 (Fig. 2a–d). However, as the temperature slowly increased throughout this period, the VOC and organic aerosol concentrations also slowly increased to reach a maximum on 21–22 July. During period 3, the organic aerosol was again dominated by alkane and carboxylic acid groups, similar to period 1, and the non-acid carbonyl concentrations were lower than those observed during period 2 at the two sites. The alcohol group fraction at Raven's Nest was significantly lower than during period 2, with the exception of 21–22 July when the alcohol concentration reached 1.5  $\mu\text{g m}^{-3}$ . At Raven's Nest, the elemental concentrations of dust



from Whistler Peak and Raven's Nest. Solutions including 2–6 factors were investigated, and a range of  $f_{\text{peak}}$  values from  $-1$  to  $1$  were used, varied in steps of  $0.2$ . Figure 3 shows how the ratio  $Q/Q_{\text{expected}}$  (Ulbrich et al., 2009) depended on numbers of factors, and on  $f_{\text{peak}}$  value, at the two sites. For solutions with five or six factors, two or more factors were not linearly independent. Furthermore, for solutions including more than four factors, one factor or more contributed less than 5 % to the total organic mass. No source could be identified for these small contributions. Therefore solutions with five factors or more were excluded, and a 4-factor solution was chosen for this study.

Figure 4 shows the four-factor solutions chosen for Whistler Peak and Raven's Nest. Each factor at Raven's Nest has a parallel factor at Whistler Peak with a rather similar spectrum (Fig. 4a–d). Factor A (Fig. 4a) has the strong and characteristic ammonium absorbance with broad double peaks in the  $2800\text{--}3400\text{ cm}^{-1}$  region that is observed for the anthropogenic combustion factors (Gilardoni et al., 2007; Hawkins et al., 2010; Takahama et al., 2011). A large fraction of factor A is comprised of alkane groups, 50 % at Whistler Peak (Fig. 4e) and 49 % at Raven's Nest (Fig. 4i); contributions from non-acid carbonyl and amine groups are low. Factor A was correlated to XRF sulfur with an  $r$ -coefficient of  $0.77$  at Whistler Peak (Table 1a), and  $0.47$  at Raven's Nest (Table 1b), which indicates that this factor is associated with fossil fuel combustion. Factor A was also correlated to  $\text{NO}_x$  at Raven's Nest ( $r = 0.74$ ) (Table 1b). At Whistler Peak, the correlation to  $\text{NO}_x$  is much weaker (Table 1a), suggesting that the combustion factor had a higher contribution from local combustion at Raven's Nest than at Whistler Peak, and a higher contribution from long-range transport at Whistler Peak than at Raven's Nest. Factor A is not correlated to any of the VOCs in Table 1 indicating low influence from biogenic VOCs (and acetonitrile) both at Whistler Peak and at Raven's Nest. We will refer to factor A as a “combustion factor”.

Factor B (Fig. 4b) is strongly dominated by alcohol groups, 65 % at Whistler Peak (Fig. 4f), and 64 % at Raven's Nest (Fig. 4j). This factor has the lowest contribution from alkane groups of all the factors. The contribution from amine groups to factor B

**Temperature-dependent accumulation mode particle**

L. Ahlm et al.

Title Page

Abstract

Introduction

Conclusions

References

Tables

Figures

⏪

⏩

◀

▶

Back

Close

Full Screen / Esc

Printer-friendly Version

Interactive Discussion



is slightly higher at Raven's Nest (10 %) than at Whistler Peak (4 %), seen also in the absorbance at  $3400\text{ cm}^{-1}$  in Fig. 4b, but apart from that the factor spectra are similar at the two sites. At Raven's Nest, factor B showed high correlation to XRF dust elements such as Fe, Al, Mg, and Mn (Table 1b). Factor B was likely associated with vegetative detritus (e.g. Rogge et al., 1993; Hildemann et al., 1996), which may be co-emitted with dust. The large fraction of alcohol groups in this factor is consistent with carbohydrate elements in plant materials (Bianchi et al., 1993). Liu et al. (2012) applied PMF to FTIR submicron organic aerosol spectra sampled in Bakersfield, CA, and found that one factor rich in alcohol (71 %) was correlated to the dust elements Si, Al, and Ca. They associated that PMF factor with vegetative detritus that resuspended with dust particles.

The hypothesis that factor B is associated with vegetative detritus is strengthened by the fact that factor B was correlated to phosphorus at both Raven's Nest (Table 1b) and Whistler Peak (Table 2a). Phosphorus is present in fluids circulating in plants and is an element associated with primary organic particles (Artaxo and Hansson, 1995; Artaxo et al., 1998). Factor B showed much lower correlation to the dust elements Fe, Al, Mg, and Mn at Whistler Peak (Table 1a) than at Raven's Nest (Table 1b). This can be explained by the fact that there is little vegetation and generally little biogenic material on the ground around the Whistler Peak site, compared to the areas around Raven's Nest. Therefore, local emission of dust at Whistler Peak did not result in any co-emission of vegetative detritus. Hence, most of the vegetative detritus associated with factor B was likely transported to the peak site from lower altitudes. Factor B will be referred to as a "detritus factor".

The PMF spectra representing factor C (Fig. 4c) strongly resemble the biogenic factor from the Whistler PMF analysis by Schwartz et al. (2010). Factor C was correlated with several of the PTR-MS gas-phase organic compounds like acetic acid/glycoaldehyde, acetone, formic acid, and methanol at Whistler Peak (Table 1a) and at Raven's Nest (Table 1b). Factor C was also mildly correlated to the biogenic tracers MVK/MACR, isoprene and monoterpenes, as well as temperature. The correlation

---

## Temperature-dependent accumulation mode particle

L. Ahlm et al.

---

[Title Page](#)[Abstract](#)[Introduction](#)[Conclusions](#)[References](#)[Tables](#)[Figures](#)[Back](#)[Close](#)[Full Screen / Esc](#)[Printer-friendly Version](#)[Interactive Discussion](#)

to temperature is logical because emissions of VOCs are temperature dependent (e.g. Guenther et al., 1993). Hence, factor C is associated with biogenic SOA.

The PMF spectra representing factor D resembles the biomass burning spectrum in Hawkins and Russell et al. (2010), with high absorbance in the alkane region and low absorbance in the alcohol region, but without the pair of methylene peaks at 2920 and 2850  $\text{cm}^{-1}$  which were observed and suggested to originate from repeating methylene units in long-chain plant cuticle wax detritus commonly observed as part of biomass burning emissions (Hawkins and Russell, 2010). The correlation to acetonitrile was also lower for factor D than for factor C at Whistler Peak (and similar at Raven's Nest). Therefore, we have no reason to believe that factor D would be dominated by biomass burning aerosol in this study. This conclusion is strengthened by the fact that factor D showed higher correlation to temperature and to BVOCs, including monoterpene and isoprene, than factor C. Thus, factor D seems to also be associated with biogenic SOA.

Factor C and factor D were weakly correlated to each other at Whistler Peak ( $r = 0.31$ ) and mildly correlated at Raven's Nest ( $r = 0.51$ ). Due to this fact, and because these factors are correlated to similar compounds, we have chosen to combine factor C and factor D to one factor that seems to be dominated by biogenic SOA. This combined factor will be referred to as a "biogenic factor". However, it cannot be excluded that the biogenic factor had some potential influence from biomass burning during the last days of the campaign, when there were some high peaks in acetonitrile concentration and smoke associated with regional fires was visible (Macdonald et al., 2012).

The detritus factor was mildly correlated to factor C ( $r = 0.50$ ) and factor D ( $r = 0.51$ ) at Raven's Nest. However, there were no corresponding correlations at Whistler Peak ( $r = 0.13$  and  $r = 0.15$ , respectively). Therefore, we have chosen to not combine the detritus factor with the biogenic factor but instead to keep it as an independent factor. This decision is also motivated by the fact that the organic functional group composition of the detritus factor strongly differ from the compositions of factors C and D (Fig. 4).

**Temperature-dependent accumulation mode particle**

L. Ahlm et al.

Title Page

Abstract

Introduction

Conclusions

References

Tables

Figures



Back

Close

Full Screen / Esc

Printer-friendly Version

Interactive Discussion



## Temperature-dependent accumulation mode particle

L. Ahlm et al.

Title Page

Abstract

Introduction

Conclusions

References

Tables

Figures

⏪

⏩

◀

▶

Back

Close

Full Screen / Esc

Printer-friendly Version

Interactive Discussion

The contribution from each of the three final factors during the campaign can be seen in the time series in Fig. 2h–i for Whistler Peak and Raven’s Nest, respectively. The sum of the PMF factors for each sample closely matches the sum of the organic functional groups seen in Fig. 2a–b for both sites. In general, the combustion factor concentration was higher at Raven’s Nest than at the Whistler Peak site. This might again indicate that a significant fraction of the anthropogenic impact on the organic aerosol at Raven’s Nest was from local sources, such as activities on the mountain or at Whistler Village in the valley.

Figure 5 shows the average contribution from each of the three PMF factors at the two sites during the whole campaign, and for the four sub-periods discussed in Sect. 3.1. Over the range of the whole campaign, the biogenic factor dominated the submicron organic aerosol mass at both sites. During the cold and humid period 1, the combustion factor dominated at Raven’s Nest. At Whistler Peak, on the other hand, the combustion factor made up the same fraction as the biogenic factor (Fig. 5). However, both the combustion factor and the biogenic factor were considerably lower at Whistler Peak than at Raven’s Nest in concentration (Fig. 2h–i). The contribution from the detritus factor was low at Raven’s Nest during period 1. The higher fraction of detritus at Whistler Peak is probably irrelevant since most of the detritus during period 1 comes from one single filter (Fig. 2h) sampled on 21–24 June (since the FTIR time resolution was low in the beginning of the campaign at the peak site).

During the warm and dry period 2, the contribution from the biogenic factor increased at both sites (Fig. 5), in particular at the Whistler Peak site where it strongly dominated (83%). The detritus fraction at Raven’s Nest was considerably higher during period 2 as a result of the very dry conditions during this period. The detritus factor made a much lower contribution at Whistler Peak than at Raven’s Nest. Period 3 had higher influence from combustion than what was the case during period 2, but the biogenic factor still dominated at both sites. In period 4, the influence from combustion was lower than during period 3, and the dominance from the biogenic factor was large, possibly then with some significant impact from biomass burning.

### 3.3 Single particle analysis using STXM-NEXAFS

In total, 47 particles were analyzed using STXM-NEXAFS. Two samples were from the Whistler Peak site and four from Raven's nest (Table 2). All samples were collected in daytime during the warm and dry period 2, when the influence from biogenic sources was high and the influence from combustion sources was at a minimum according to the PMF factor contributions in Fig 5. Most of the sampled particles were in the size range of 1–5  $\mu\text{m}$  diameters.

The carboxylic acid group was the most dominant functional group in the analyzed samples, and was more pronounced at the Whistler Peak site compared to Raven's nest (Fig. 6). There were several particles at both sites with the carboxylic peak being several times larger than the other peaks. An example of such a particle with its absorbance is shown in Fig. 7. The dominance of the carboxylic acid group might suggest a large fraction of SOA in the analyzed particles. Other functional groups such as alkyl, alcohol, and inorganic carbonate showed higher variability. Alkene, aromatic and ketonic groups made a lower contribution compared to other functional groups.

At Whistler Peak during summer 2009, Takahama et al. (2011) observed large contributions from ketonic carbonyl and alkene/aromatic groups and attributed it to the influence from carbon tarballs produced during biomass burning events. However, during period 2 in this study, biogenic sources dominated and the acetonitrile concentrations stayed low, indicating low influence from biomass burning. Many of the single particles at both sites in Whistler had similar spectral features to SOA generated inside a smog chamber from  $\alpha$ -pinene (with or without isoprene), but none of the single particles collected at Whistler were similar to the SOA formed from 1,2,4-trimethylbenzene, an SOA precursor emitted from combustion sources (Shakya et al., 2012). These results corroborate with the large biogenic source for period 2 (Fig. 5) obtained from the PMF analysis and the contrast from previous study during 2009.

Based on cluster analyses (Takahama et al., 2007) of single particles analyzed by STXM-NEXAFS, Schwartz et al. (2010) found that a majority of their spectra were of

## Temperature-dependent accumulation mode particle

L. Ahlm et al.

Title Page

Abstract

Introduction

Conclusions

References

Tables

Figures



Back

Close

Full Screen / Esc

Printer-friendly Version

Interactive Discussion



particle types “secondary” and “other” at Whistler during summer 2008. The cluster analyses in this study also gave the result that most particles were of the type “SOA”, and more so at Whistler Peak ( $\sim 2/3$ ) compared to Raven’s Nest ( $\sim 1/2$ ). Other particle types at Whistler Peak were soil dust, and at Raven’s nest biomass burning, combustion, and soil dust. These results are again consistent with the PMF results with a larger biogenic contribution at Whistler Peak (83 %) than at Raven’s Nest (48 %) during period 2 (Fig. 5).

### 3.4 Links between particle number concentration, CCN and the PMF factors

In Sects. 3.1–3.2, the focus was on the organic mass and sources responsible for the organic mass. In this section, the focus will also be on the origins of the particle and CCN number concentrations as well as their associations. In particular during period 3 (13–22 July), there were strong diurnal variations in VOC concentrations (Fig. 2c–d) and aerosol concentrations (Fig. 2g). Figure 8 shows median diurnal cycles of concentrations of total particle number,  $\text{SO}_2$ ,  $\text{NO}_x$ , and BC during period 3 at the two sites. In addition, median diurnal cycles of the ratios of the non-oxygenated AMS ion fragment  $\text{C}_4\text{H}_9^+$  and the oxygenated ion fragment  $\text{CO}_2^+$  to total organic aerosol concentration at Raven’s Nest can be seen in Fig. 8. The AMS mass spectral peak  $m/z$  57 contains the ion peaks  $\text{C}_4\text{H}_9^+$  and  $\text{C}_3\text{H}_5\text{O}^+$ , and  $m/z$  44 contains the ion peaks  $\text{CO}_2^+$  and  $\text{C}_2\text{H}_4\text{O}^+$ . Since the ion fragments of a certain  $m/z$  measured by the C-ToF-AMS used at Whistler Peak cannot be separated, we have instead included the median diurnal cycles of the ratios of  $m/z$  57 and  $m/z$  44 to total organic aerosol concentration for the Whistler Peak site in Fig. 8.

At Raven’s Nest, there was a very pronounced peak in  $\text{NO}_x$  around 10:00 h (Fig. 8c). This was likely a combined result of emissions from overnight and morning traffic in Whistler and the growing mixed layer reaching the altitude of Raven’s Nest. At the same time, the particle number (Fig. 8a) and BC (Fig. 8d) concentrations also exhibited small peaks. For the  $\text{C}_4\text{H}_9^+$ -ratio (Fig. 8e), there is a slight and broad increase during the daytime visible at least in the third quartile, with broad similarity to the BC pattern. The

## Temperature-dependent accumulation mode particle

L. Ahlm et al.

Title Page

Abstract

Introduction

Conclusions

References

Tables

Figures



Back

Close

Full Screen / Esc

Printer-friendly Version

Interactive Discussion



CO<sub>2</sub><sup>+</sup>-ratio (Fig. 8f) stayed more constant during the day. Due to the morning correlation of particle number with NO<sub>x</sub> and BC at Raven's Nest, the slight peak in particle number concentration around 10:00 h was likely due to primary aerosol particles emitted from local sources. Corresponding morning peaks were less evident at the Whistler Peak site (Fig. 8g, i, j, and k), likely because the mixed layer in general reached the level of the mountain peak in the afternoon when the layer had been more diluted during growth.

In the evening, between 18:00 h and 20:00 h, the particle number concentration at Raven's Nest (Fig. 8a) had a second more pronounced peak. That was about the same time as the particle number concentration peaked at Whistler Peak (Fig. 8g). The BC concentration at Raven's Nest (Fig. 8d) also experienced a second maximum in the evening, similar to the particle number concentration. This evening BC peak was very pronounced at the Whistler Peak site as well (Fig. 8j). The fact that particle number and BC peaked at the same time in the evening at the two sites suggests that this peak was at least partly a result of anthropogenic sources. Also SO<sub>2</sub> experienced a maximum in the evening (Fig. 8b and h).

The average total particle number concentrations over the whole campaign were 2290 and 1210 cm<sup>-3</sup> at Raven's Nest and Whistler Peak, respectively. Table 3 shows median particle number concentrations for each of the four periods separately at the two sites. During period 1, the median number concentration at Raven's Nest was almost a factor of three higher than the corresponding concentration at Whistler Peak. This relative difference between the two sites was larger during period 1 than during the other three periods, likely as a result of occasional decoupling between the sometimes existing cloud layer at Whistler Peak with the boundary layer during period 1.

Figure 9 includes time series of the integrated SMPS particle number size distribution (Fig. 9a), concentrations of total particle number and NO<sub>x</sub> (Fig. 9b), particle number concentrations in the particle diameter intervals 16–100 nm ( $N_{16-100}$ ) and 100–700 nm ( $N_{100}$ ) (Fig. 9c), and the PMF organic combustion and biogenic factors (Fig. 9d), at Raven's Nest. The particle number concentration followed the NO<sub>x</sub> concentration

**Temperature-dependent accumulation mode particle**

L. Ahlm et al.

Title Page

Abstract

Introduction

Conclusions

References

Tables

Figures

⏪

⏩

◀

▶

Back

Close

Full Screen / Esc

Printer-friendly Version

Interactive Discussion



---

**Temperature-dependent accumulation mode particle**

---

L. Ahlm et al.

[Title Page](#)[Abstract](#)[Introduction](#)[Conclusions](#)[References](#)[Tables](#)[Figures](#)[⏪](#)[⏩](#)[◀](#)[▶](#)[Back](#)[Close](#)[Full Screen / Esc](#)[Printer-friendly Version](#)[Interactive Discussion](#)

somewhat during period 1 (Fig. 9b), particularly between 28 June and 5 July. However, the peaks in number concentration during the evenings on 24 June and 26 June (Fig. 9b) and growth from small sizes (Fig. 9a) could be results of nucleation events since  $\text{NO}_x$  (Fig. 9b) and  $N_{100}$  (Fig. 9c) remained low during these two growth events.

5 There is no correlation between particle number and  $\text{SO}_2$  during period 1 at Raven's Nest (Table 4). However,  $r$ -coefficients between total particle number and  $\text{NO}_x$ , BC, and CO are in the range 0.49–0.62 for Raven's Nest (Table 4) suggesting a significant contribution to the particle numbers from anthropogenic sources during period 1. At Whistler Peak, there are no such corresponding correlations, which again suggest that  
10 the Whistler Peak site was at times decoupled from the boundary layer during period 1.

Period 2 started with two very clear nucleation events on 5 July and 6 July (Fig. 9a) which have been described in detail by Pierce et al. (2012). Period 2 had the lowest  $\text{NO}_x$  concentration (Fig. 9b) and the lowest PMF combustion factor concentration (Fig. 9d) of all the periods. The  $r$ -coefficients between number concentration and  $\text{NO}_x$ , BC, and  
15 CO, are in general low or negative at both Raven's Nest and Whistler Peak during period 2 (Table 4), indicating low contribution from primary emissions. Hence, it appears that new particle formation largely dominated the particle number concentration during period 2. Total particle number concentrations are moderately correlated to  $\text{SO}_2$  ( $r = 0.62$ ) at Raven's Nest during period 2, but there is no such correlation at Whistler  
20 Peak, which could indicate that nucleation preferably occurred at lower altitudes.

BC number concentrations were higher during period 3 than during period 2 (Table 3). Furthermore, the  $r$ -coefficients between particle number and BC are also higher during period 3 than during period 2 (Table 4). High peaks in both number concentration and  $\text{NO}_x$  can be seen around midnight between 11 and 12 July (Fig. 9b), suggesting a plume of primary particles at that time. The  $r$ -coefficient between particle number and  
25  $\text{SO}_2$  is lower during period 3 than during period 2 at Raven's Nest, suggesting that new particle formation from gas-phase oxidation of  $\text{SO}_2$  contributed less during period 3 than during period 2.

Period 4 started with a very clear nucleation event in the afternoon of 22 July (Fig. 9a). There was a rapid increase in particle number and a simultaneous drop in  $\text{NO}_x$  concentration during this event (Fig. 9b), and at the same time the number of accumulation mode particles remained low. Despite this nucleation event, period 4 has the highest correlations between particle number and BC, CO, and  $\text{NO}_x$ , all in the range 0.43–0.89 (Table 4), indicating significant contributions from anthropogenic sources and/or biomass burning to the aerosol particle population; the higher BC concentrations during period 4 (Table 3) suggest a biomass burning contribution. This hypothesis is supported by observed large peaks in acetonitrile during the same time period.

Comparing Fig. 9c and d, it can be seen that  $N_{16-100}$  follows the mass concentrations of the PMF combustion factor relatively well.  $N_{16-100}$  is correlated with the combustion factor ( $r = 0.40$ ) at Raven's Nest, but with neither the biogenic factor ( $r = -0.20$ ) nor the detritus factor ( $r = -0.29$ ). Hence, many of the particles smaller than 100 nm at Raven's Nest were likely related to combustion sources. This does not imply that the combustion factor mass was dominated by ultrafine particles since fossil fuel combustion also emits particles that are larger than 100 nm.

Whereas  $N_{16-100}$  follows the combustion factor in Fig. 9c–d relatively well as discussed above,  $N_{100}$  follows the concentration of the PMF biogenic factor. The associated  $r$ -coefficient for correlation between  $N_{100}$  and the biogenic factor is 0.88 and 0.83 at Raven's Nest and Whistler Peak, respectively. There are no such clear correlations between  $N_{100}$  and the combustion factor ( $r = -0.01$  and  $r = -0.15$ ), or the detritus factor ( $r = 0.56$  and  $r = -0.05$ ) at the two sites, respectively. Since the biogenic factor was largely dominated by biogenic SOA throughout most of the campaign, except possibly during the last days of period 4 (Sect. 3.2), the high correlation between the biogenic factor and  $N_{100}$  suggests that the concentration of particles larger than 100 nm was controlled to a large extent by particle condensational growth from biogenic vapors. Hence, although combustion sources contributed to  $N_{16-100}$ ,  $N_{100}$  depended critically on biogenic SOA in this study.

**Temperature-dependent accumulation mode particle**

L. Ahlm et al.

Title Page

Abstract

Introduction

Conclusions

References

Tables

Figures

⏪

⏩

◀

▶

Back

Close

Full Screen / Esc

Printer-friendly Version

Interactive Discussion



---

**Temperature-dependent accumulation mode particle**

---

L. Ahlm et al.

[Title Page](#)[Abstract](#)[Introduction](#)[Conclusions](#)[References](#)[Tables](#)[Figures](#)[⏪](#)[⏩](#)[◀](#)[▶](#)[Back](#)[Close](#)[Full Screen / Esc](#)[Printer-friendly Version](#)[Interactive Discussion](#)

Many studies (e.g. Kapustin et al., 2006; Clarke et al., 2010) suggest the number concentration of particles with  $D_p > 100$  nm as a surrogate for the CCN concentration. Here we consider the scope of that assumption for a biogenic event. The correlation between the CCN concentration and the biogenic factor in general increased with increasing supersaturation (Table 5). For  $S = 0.2$ , the  $r$ -coefficient was 0.69, and for higher supersaturations the correlation was even stronger. Thus, the CCN number concentration was strongly related to the biogenic factor.

Temperature may influence the concentration of particles larger than 100 nm by increasing the emission of BVOCs. Figure 10a and b show the concentrations of particles larger than 100 nm as functions of local temperature at the two sites for the entire study.  $N_{100}$  is strongly correlated to ambient temperature at both sites which indicates that temperature was an important factor for  $N_{100}$  at both sites. Figure 10c and d show the corresponding relations for numbers of CCN for  $S = 0.2\%$  (Fig. 10c) and for  $S = 0.3\%$  (Fig. 10d) at Raven's Nest. The correlation coefficient was similar for  $S = 0.5\%$  ( $r = 0.63$ ). For  $S = 0.1\%$ , there was no correlation ( $r = 0.06$ ) between the number of CCN and temperature.

The particles here are predominantly composed of organics with some sulfate. The correlation between concentrations of particles larger than 100 nm and CCN at  $S = 0.2\%$  at Raven's Nest (Fig. 10e) is strong, however the CCN concentration at  $S = 0.2\%$  is a factor of two lower than  $N_{100}$ . Thus, in general we expect  $N_{100}$  to provide some measure of CCN at  $S = 0.2\%$  with variations of about a factor of two. We note that while the correlation of  $N_{100}$  and CCN at  $S = 0.2\%$  is strong (Fig. 10e), that of CCN at  $S = 0.2\%$  with temperature (Fig. 10c) is weaker than the  $N_{100}$  versus temperature (Fig. 10a). The weaker relationship of CCN at  $S = 0.2\%$  with temperature may be a result of different hygroscopic properties for different aerosol particles. The hygroscopicity of sulfate is higher than that of organics. Furthermore, different types of organic particles like primary detritus particles and biogenic SOA are likely to have different hygroscopic properties, and also different dependences on temperature, which may explain the weaker relation for CCN with temperature than for  $N_{100}$  with temperature.

## 4 Summary and conclusions

PMF has been applied to FTIR spectra in order to investigate and quantify sources of submicron organic aerosols at Whistler Peak (2182 m a.s.l.) and Raven's Nest (1300 m a.s.l.) during the WACS 2010 campaign at Whistler Mountain, British Columbia. Here the key results and main conclusions are presented:

- The factors that could be identified at the two sites are: (1) a combustion factor, (2) a biogenic factor, and (3) a vegetative detritus factor.
- The combustion factor dominated the organic aerosol mass at both sites during the early part of the campaign, which was characterized by low temperatures and advection from the Vancouver area. However, as the temperature started to rise in early July, the biogenic factor increased as a result of increased emissions of BVOCs, and came to be the largest factor throughout the rest of the campaign.
- The largest difference between the two sites in terms of organic aerosol composition was the much higher concentration of alcohol functional groups at Raven's Nest than at Whistler Peak during the dry mid-part of the campaign. These alcohol groups were likely associated with local emissions of vegetative detritus. The lower fraction of detritus at Whistler Peak was a result of a snow covered surface at the peak of the mountain, and also little vegetation up there.
- On average over the whole campaign, the biogenic factor represented 69 % and 49 %, the combustion factor represented 14 % and 23 %, and the detritus factor represented 17 % and 27 % at Whistler Peak and Raven's Nest, respectively. The larger fraction of combustion at Raven's Nest compared to Whistler Peak was likely a result of some local pollution from Whistler Village in the valley.

The biogenic factor was correlated to temperature and to several VOCs. The number concentration of particles with  $D_p > 100$  nm was strongly correlated to the biogenic factor (and to temperature), whereas the number concentration of particles smaller than

28010

ACPD

12, 27989–28031, 2012

### Temperature-dependent accumulation mode particle

L. Ahlm et al.

Title Page

Abstract

Introduction

Conclusions

References

Tables

Figures

⏪

⏩

◀

▶

Back

Close

Full Screen / Esc

Printer-friendly Version

Interactive Discussion



100 nm was better correlated to the combustion factor. CCN data from Raven's Nest showed that the CCN concentration was correlated to temperature and to the biogenic factor for supersaturations equal to or larger than 0.2 %. This is an indication that temperature and biogenic SOA formation exerted a large control on the CCN population for supersaturations equal to or larger than 0.2 % during this study.

*Acknowledgements.* Environment Canada funded the Whistler Aerosol and Cloud Study 2010 through the Clean Air Regulatory Agenda (CARA). Funding was provided through Environment Canada's Grants and Contribution program. Co-operation and support from Whistler-Blackcomb and Juniper Buller is gratefully acknowledged. We would also like to thank D. J. Cziczko for providing CCN data.

## References

- Artaxo, P. and Hansson H.-C.: Size distribution of biogenic aerosol particles from the Amazon Basin, *Atmos. Environ.*, 29, 393–402, 1995.
- Artaxo, P., Fernandes, E. T., Martins, J. V., Yamasoe, M. A., Hobbs, P. V., Maenhaut, W., Longo, K. M., and Castanho, A.: Large-scale aerosol source apportionment in Amazonia, *J. Geophys. Res.*, 103, 31837–31847, 1998.
- Bianchi, G., Gamba, A., Limioli, R., Pozzi, N., Elster, R., Salamini, F., and Bartels, D.: The unusual sugar composition in leaves of the resurrection plant *myrothamnus-flabellifolia*, *Physiol. Plantarum*, 87, 223–226, 1993.
- Clarke, A. and Kapustin, V.: Hemispheric aerosol vertical profiles: Anthropogenic impacts on optical depth and cloud nuclei, *Science*, 329, 1488–1492, 2010.
- DeCarlo, P. F., Kimmel, J. R., Trimborn, A., Northway, M. J., Jayne, J. T., Aiken, A. C., Gonin, M., Fuhrer, K., Horvath, T., Docherty, K. S., Worsnop, D. R., and Jimenez, J. L.: Field-Deployable, High-Resolution, Time-of-flight Aerosol Mass Spectrometer, *Anal. Chem.*, 78, 8281–8289, 2006.
- Drewnick, F., Hings, S. S., DeCarlo, P., Jayne, J. T., Gonin, M., Fuhrer, K., Weimer, S., Jimenez, J. L., Demerjian, K. L., Borrmann, S., and Worsnop, D. R.: A New Time-of-Flight Aerosol Mass Spectrometer (ToF-AMS)-Instrument Description and First Field Deployment, *Aerosol Sci. Tech.*, 39, 637–658, 2005.

## Temperature-dependent accumulation mode particle

L. Ahlm et al.

Title Page

Abstract

Introduction

Conclusions

References

Tables

Figures

⏪

⏩

◀

▶

Back

Close

Full Screen / Esc

Printer-friendly Version

Interactive Discussion



## Temperature-dependent accumulation mode particle

L. Ahlm et al.

[Title Page](#)
[Abstract](#)
[Introduction](#)
[Conclusions](#)
[References](#)
[Tables](#)
[Figures](#)
[⏪](#)
[⏩](#)
[◀](#)
[▶](#)
[Back](#)
[Close](#)
[Full Screen / Esc](#)
[Printer-friendly Version](#)
[Interactive Discussion](#)

- Frossard, A. A., Shaw, P. M., Russell, L. M., Kroll, J. H., Canagratna, M. R., Worsnop, D. R., Quinn, P. K., and Bates, T. S.: Springtime Arctic haze contributions of submicron organic particles from European and Asian combustion sources, *J. Geophys. Res.*, 116, D05205, doi:10.1029/2010JD015178, 2011.
- 5 Gilardoni, S., Russell, L. M., Sorooshian, A., Flagan, R. C., Seinfeld, J. H., Bates, T. S., Quinn, P. K., Allan, J. D., Williams, B., Goldstein, A. H., Onasch, T. B., and Worsnop, D. R.: Regional variations of organic functional groups in aerosol particles on four U.S. east coast platforms during the International Consortium for Atmospheric Research on Transport and Transformation 2004 campaign, *J. Geophys. Res.*, 112, D10S27, doi:10.1029/2006JD007737, 2007.
- 10 Goldstein, A. H. and Galbally, I. E.: Known and unexplored organic constituents in the earth's atmosphere, *Environ. Sci. Technol.*, 41, 1514–1521, 2007.
- Guenther, A. B., Zimmerman, P. R., Harley, P. C., Russell, K. M., and Fall, R.: Isoprene and monoterpene emission rate variability: Model evaluations and sensitivity analyses, *J. Geophys. Res.*, 98, 12609–12617, doi:10.1029/93JD00527, 1993.
- 15 Hallquist, M., Wenger, J. C., Baltensperger, U., Rudich, Y., Simpson, D., Claeys, M., Dommen, J., Donahue, N. M., George, C., Goldstein, A. H., Hamilton, J. F., Herrmann, H., Hoffmann, T., Iinuma, Y., Jang, M., Jenkin, M. E., Jimenez, J. L., Kiendler-Scharr, A., Maenhaut, W., McFiggans, G., Mentel, Th. F., Monod, A., Prévôt, A. S. H., Seinfeld, J. H., Surratt, J. D., Szmigielski, R., and Wildt, J.: The formation, properties and impact of secondary organic aerosol: current and emerging issues, *Atmos. Chem. Phys.*, 9, 5155–5236, doi:10.5194/acp-9-5155-2009, 2009.
- 20 Hawkins, L. N. and Russell, L. M.: Oxidation of ketone groups in transported biomass burning aerosol from the 2008 Northern California Lightning Series fires, *Atmos. Environ.*, 44, 4142–4154, 2010.
- 25 Hawkins, L. N., Russell, L. M., Covert, D. S., Quinn, P. K., and Bates, T. S.: Carboxylic acids, and sulfates, and organosulfates in processed continental organic aerosol over the southeast Pacific Ocean during VOCALS-Rex 2008, *J. Geophys. Res.*, 115, D13201, doi:10.1029/2009JD013276, 2010.
- 30 Hildemann, L. M., Rogge, W. F., Cass, G. R., Mazurek, M. A., and Simoneit, B. R. T.: Contribution of primary aerosol emissions from vegetation-derived sources to fine particle concentrations in Los Angeles, *J. Geophys. Res.*, 101, 19541–19549, doi:10.1029/95JD02136, 1996.

---

**Temperature-dependent accumulation mode particle**

---

L. Ahlm et al.

[Title Page](#)[Abstract](#)[Introduction](#)[Conclusions](#)[References](#)[Tables](#)[Figures](#)[⏪](#)[⏩](#)[◀](#)[▶](#)[Back](#)[Close](#)[Full Screen / Esc](#)[Printer-friendly Version](#)[Interactive Discussion](#)

- Hitchcock, A. P.: aXis2000 Software Version 2.0c, Hitchcock Group, McMaster University, Hamilton, Ont., Canada, 2000.
- Jimenez, J. L., Canagaratna, M. R., Donahue, N. M., Prevot, A. S. H., Zhang, Q., Kroll, J. H., DeCarlo, P. F., Allan, J. D., Coe, H., Ng, N. L., Aiken, A. C., Docherty, K. S., Ulbrich, I. M., Grieshop, A. P., Robinson, A. L., Duplissy, J., Smith, J. D., Wilson, K. R., Lanz, V. A., Hueglin, C., Sun, Y. L., Tian, J., Laaksonen, A., Raatikainen, T., Rautiainen, J., Vaattovaara, P., Ehn, M., Kulmala, M., Tomlinson, J. M., Collins, D. R., Cubison, M. J., Dunlea, E. J., Huffman, J. A., Onasch, T. B., Alfarra, M. R., Williams, P. I., Bower, K., Kondo, Y., Schneider, J., Drewnick, F., Borrmann, S., Weimer, S., Demerjian, K., Salcedo, D., Cottrell, L., Griffin, R., Takami, A., Miyoshi, T., Hatakeyama, S., Shimono, A., Sun, J. Y., Zhang, Y. M., Dzepina, K., Kimmel, J. R., Sueper, D., Jayne, J. T., Herndon, S. C., Trimborn, A. M., Williams, L. R., Wood, E. C., Middlebrook, A. M., Kolb, C. E., Baltensperger, U., and Worsnop, D. R.: Evolution of Organic Aerosols in the Atmosphere, *Science*, 326, 1525–1529, 2009.
- Kapustin, V. N., Clarke, A. D., Schinozuka, Y., Howell, S., Brekhovskikh, V., Nakajima, T., and Higurashi, A.: On the determination of a cloud condensation nuclei from satellite: Challenges and possibilities, *J. Geophys. Res.*, 111, D04202, doi:10.1029/2004JD005527, 2006.
- Kilcoyne, A. L. D., Tyliszczak, T., Steele, W. F., Fakra, S., Hitchcock, P., Franck, K., Anderson, E., Harteneck, B., Rightor, E. G., Mitchell, G. E., Hitchcock, A. P., Yang, L., Warwick, T., and Ade, H.: Interferometer controlled scanning transmission X-ray microscopes at the advanced light source, *J. Synchrotron Rad.*, 10, 125–136, 2003.
- Leaïch, W. R., Macdonald, A. M., Brickell, P. C., Liggio, J., Sjostedt, S. J., Vlasenko, A., Bottenheim, J. W., Huang, L., Li, S. –M., Liu, P. S. K., Toom-Saunty, D., Hayden, K. A., Sharma, S., Schantz, N. C., Wiebe, H. A., Zhang, W., Abbatt, J. P. D., Slowik, J. G., Chang, R. Y. –W., Russell, L. M., Schwartz, R. E., Takahama, S., Jayne, J. T., and Ng, N. L.: Temperature response of the submicron organic aerosol from temperate forests, *Atmos. Environ.*, 45, 6696–6704, 2011.
- Liu, S., Day, D. A., Shields, J. E., and Russell, L. M.: Ozone-driven daytime formation of secondary organic aerosol containing carboxylic acid groups and alkane groups, *Atmos. Chem. Phys.*, 11, 8321–8341, doi:10.5194/acp-11-8321-2011, 2011.
- Liu, S., Ahlm, L., Day, D. A., Russell, L. M., Zhao, Y., Gentner, D. R., Weber, R., Goldstein, A. H., Jaoui, M., Offenberg, J. H., Kleindienst, T. E., Rubitschun, C., Surratt, J. D., Sheesley, R. J., and Scheller, S.: Secondary organic aerosol formation from fossil fuel

---

## Temperature-dependent accumulation mode particle

L. Ahlm et al.

---

Title Page

Abstract

Introduction

Conclusions

References

Tables

Figures



Back

Close

Full Screen / Esc

Printer-friendly Version

Interactive Discussion

sources contribute majority of summertime organic mass at Bakersfield, *J. Geophys. Res.*, doi:10.1029/2012JD018170, in press, 2012.

Macdonald, A. M., Leaitch, W. R., Abbatt, J. P. D., Ahlm L., Al-Basheer, W., Betram, A. K., Buller, J., Campuzano-Jost, P., Chan, E., Corbin, J., Cziczo, D. J., Elford, A., Hayden, K. L., Herckes, P., Lee, A. K. Y., Li, S. -M., Liggio, J., Liu, P. S. K., Mihele, C., Noone, K. J., Pierce, J. R., Russell, L. M., Toom-Sauntry, D., Schroder, J., Sharma, S., Sheppard, A., Sjostedt, S. J., Slowik, J. G., Strawbridge, K., Stuppel, G., Vlasenko, A., Wainwright, C. D., Wang, Y., Wentzell, J., Allan Wiebe, H., and Wong, J. P. S.: Overview of WACS 2010: Biogenic Aerosol Formation, Mountain Flows and CCN, *Atmos. Chem. Phys. Discuss.*, in preparation, 2012.

Maria, S. F., Russell, L. M., Turpin, B. J., Porcja, R. J., Campos, T. L., Weber, R. J., and Huebert, B. J.: Source signatures of carbon monoxide and organic functional groups in Asian Pacific Regional Aerosol Characterization Experiment (ACE-Asia) submicron aerosol types, *J. Geophys. Res.*, 108, 8637, 5–1 to 5–14, doi:10.1029/2003JD003703, 2003.

Paatero, P. and Tapper, U.: Positive Matrix Factorization: A non-negative factor model with optimal utilization of error estimates of data values, *Environmetrics*, 5, 111–126, doi:10.1002/env.3170050203, 1994.

Pierce, J. R., Leaitch, W. R., Liggio, J., Westervelt, D. M., Wainwright, C. D., Abbatt, J. P. D., Ahlm, L., Al-Basheer, W., Cziczo, D. J., Hayden, K. L., Lee, A. K. Y., Li, S.-M., Russell, L. M., Sjostedt, S. J., Strawbridge, K. B., Travis, M., Vlasenko, A., Wentzell, J. J. B., Wiebe, H. A., Wong, J. P. S., and Macdonald, A. M.: Nucleation and condensational growth to CCN sizes during a sustained pristine biogenic SOA event in a forested mountain valley, *Atmos. Chem. Phys.*, 12, 3147–3163, doi:10.5194/acp-12-3147-2012, 2012.

Roberts, G. C., Nenes, A., Seinfeld, J. H., and Andreae, M. O.: Impact of biomass burning on cloud properties in the Amazon Basin, *J. Geophys. Res.*, 108, 4062, 9–1 to 9–19, doi:10.1029/2001JD000985, 2003.

Rogge, W. F., Hildemann, L. M., Mazurek, M. A., Cass, G. R., and Simoneit, B. R. T.: Sources of fine organic aerosol. 4. Particulate abrasion products from leaf surfaces of urban plants, *Environ. Sci. Technol.*, 27, 2700–2711, 1993.

Russell, L. M., Takahama, S., Liu, S., Hawkins, L. N., Covert, D. S., Quinn, P. K., and Bates, T. S.: Oxygenated fraction and mass of organic aerosol from direct emission and atmospheric processing measured on the R/V Ronald Brown during TEXAQS/GoMACCS 2006, *J. Geophys. Res.*, 114, D00F05, doi:10.1029/2008JD011275, 2009.

---

**Temperature-dependent accumulation mode particle**

---

L. Ahlm et al.

[Title Page](#)[Abstract](#)[Introduction](#)[Conclusions](#)[References](#)[Tables](#)[Figures](#)[⏪](#)[⏩](#)[◀](#)[▶](#)[Back](#)[Close](#)[Full Screen / Esc](#)[Printer-friendly Version](#)[Interactive Discussion](#)

Schwartz, R. E., Russell, L. M., Sjostedt, S. J., Vlasenko, A., Slowik, J. G., Abbatt, J. P. D., Macdonald, A. M., Li, S. M., Liggio, J., Toom-Sauntry, D., and Leaitch, W. R.: Biogenic oxidized organic functional groups in aerosol particles from a mountain forest site and their similarities to laboratory chamber products, *Atmos. Chem. Phys.*, 10, 5075–5088, doi:10.5194/acp-10-5075-2010, 2010.

Shakya, K. M., Liu, S., Takahama, S., Russell, L. M., Keutsch, F. N., Galloway, M. M., Shilling, J. E., Hiranuma, N., Song, C., Kim, H., Paulson, S. E., Pfaffenberger, L., Barmet, P., Slowik, J., Prevot, A. S. H., Dommen, J., Baltensperger, U.: Similarities in STXM-NEXAFS spectra of atmospheric particles and secondary organic aerosol generated from glyoxal, alpha-pinene, isoprene, 1,2,4-trimethylbenzene, and d-limonene, *Aerosol Sci. Technol.*, submitted, 2012.

Takahama, S., Gilardoni, S., Russell, L. M., and Kilcoyne, A. L. D.: Classification of multiple types of organic carbon composition in atmospheric particles by scanning transmission X-ray microscopy analysis, *Atmos. Environ.*, 41, 9435–9451, 2007.

Takahama, S., Liu, S., and Russell, L. M.: Coatings and clusters of carboxylic acids in carbon-containing atmospheric particles from spectromicroscopy and their implications for cloud-nucleating and optical properties, *J. Geophys. Res.*, 115, D01202, doi:10.1029/2009JD012622, 2010.

Takahama, S., Schwartz, R. E., Russell, L. M., Macdonald, A. M., Sharma, S., and Leaitch, W. R.: Organic functional groups in aerosol particles from burning and non-burning forest emissions at a high-elevation mountain site, *Atmos. Chem. Phys.*, 11, 6367–6386, doi:10.5194/acp-11-6367-2011, 2011.

Tsigaridis, K. and Kanakidou, M.: Secondary organic aerosol importance in the future atmosphere, *Atmos. Environ.*, 41, 4682–4692, 2007.

Ulbrich, I. M., Canagaratna, M. R., Zhang, Q., Worsnop, D. R., and Jimenez, J. L.: Interpretation of organic components from Positive Matrix Factorization of aerosol mass spectrometric data, *Atmos. Chem. Phys.*, 9, 2891–2918, doi:10.5194/acp-9-2891-2009, 2009.

Wong, J. P. S., Lee, A. K. Y., Slowik, J. G., Cziczo, D. J., Leaitch, W. R., Macdonald, A., and Abbatt, J. P. D.: Oxidation of ambient biogenic secondary organic aerosol by hydroxyl radicals: Effects on cloud condensation nuclei activity, *Geophys. Res. Lett.*, 38, L22805, doi:10.1029/2011GL049351, 2011.

## Temperature-dependent accumulation mode particle

L. Ahlm et al.

**Table 1a.** *r*-coefficients between the four PMF factors and tracers at Whistler Peak. All elements, gases, and parameters in the first column have been averaged over the same time interval as the filters were sampled over.

WHI	Factor A	Factor B	Factor C	Factor D
NO <sub>x</sub>	0.26	-0.12	0.39	0.27
S	0.77	0.22	0.15	-0.10
Fe	0.06	0.17	0.90	0.17
Al	0.05	0.17	0.86	0.38
Mg	0.13	0.18	0.86	0.13
Mn	0.04	0.12	0.88	0.28
P	-0.08	0.81	0.00	-0.22
Monoterpenes	-0.46	-0.09	0.21	0.56
Isoprenes	-0.57	-0.21	0.33	0.42
MVK/MACR	-0.47	-0.19	0.66	0.69
Acetone	-0.11	-0.19	0.85	0.84
Methanol	-0.24	-0.13	0.79	0.86
Formic acid	-0.24	-0.20	0.85	0.83
Acetic acid/glycoaldehyde	-0.10	-0.35	0.93	0.47
Acetonitrile	-0.16	-0.28	0.50	0.17
Temperature	-0.34	0.09	0.52	0.74

[Title Page](#)
[Abstract](#)
[Introduction](#)
[Conclusions](#)
[References](#)
[Tables](#)
[Figures](#)
[Back](#)
[Close](#)
[Full Screen / Esc](#)
[Printer-friendly Version](#)
[Interactive Discussion](#)

## Temperature-dependent accumulation mode particle

L. Ahlm et al.

[Title Page](#)[Abstract](#)[Introduction](#)[Conclusions](#)[References](#)[Tables](#)[Figures](#)[⏪](#)[⏩](#)[◀](#)[▶](#)[Back](#)[Close](#)[Full Screen / Esc](#)[Printer-friendly Version](#)[Interactive Discussion](#)

**Table 1b.** *r*-coefficients between the four PMF factors and tracers at Raven's Nest. All elements, gases, and parameters in the first column have been averaged over the same time interval as the filters were sampled over.

WRN	Factor A	Factor B	Factor C	Factor D
NO <sub>x</sub>	0.74	−0.30	0.17	0.14
S	0.47	−0.09	0.05	0.16
Fe	−0.42	0.87	0.45	0.39
Al	−0.43	0.87	0.45	0.36
Mg	−0.36	0.86	0.39	0.27
Mn	−0.38	0.90	0.45	0.39
P	−0.30	0.78	0.39	0.05
Monoterpenes	−0.54	0.57	0.44	0.67
Isoprenes	−0.42	0.54	0.63	0.79
MVK/MACR	−0.48	0.56	0.58	0.80
Acetone	−0.36	0.63	0.63	0.78
Methanol	−0.44	0.60	0.57	0.74
Formic acid	−0.44	0.66	0.58	0.85
Acetic acid/glycoaldehyde	−0.42	0.70	0.65	0.80
Acetonitrile	−0.32	0.38	0.55	0.61
Temperature	−0.40	0.49	0.54	0.65

**Temperature-dependent accumulation mode particle**

L. Ahlm et al.

Title Page

Abstract

Introduction

Conclusions

References

Tables

Figures

I◀

▶I

◀

▶

Back

Close

Full Screen / Esc

Printer-friendly Version

Interactive Discussion

**Table 2.** Description of STXM samples.

Site	Date	Sampling time	No. of particles
WHI	9 July	14:10–15:28	4
WHI	10 July	14:52–16:02	10
WRN	5 July	14:00–15:00	3
WRN	8 July	12:42–13:20	17
WRN	9 July	11:59–12:30	10
WRN	10 July	12:23–12:53	3

## Temperature-dependent accumulation mode particle

L. Ahlm et al.

Title Page

Abstract

Introduction

Conclusions

References

Tables

Figures

◀

▶

◀

▶

Back

Close

Full Screen / Esc

Printer-friendly Version

Interactive Discussion

**Table 3.** Median concentrations of the integrated total particle number from the SMPS and BC from the SP2 during each period for the two sites.

	Site	Period 1	Period 2	Period 3	Period 4
Total number concentration ( $\text{cm}^{-3}$ )	WHI	690	1500	1210	1570
	WRN	1980	2180	2540	2620
SP2 number concentration ( $\text{cm}^{-3}$ )	WHI	5.75	7.85	8.68	25.3
	WRN	7.05	3.57	6.39	7.78

## Temperature-dependent accumulation mode particle

L. Ahlm et al.

Title Page

Abstract

Introduction

Conclusions

References

Tables

Figures

⏪

⏩

◀

▶

Back

Close

Full Screen / Esc

Printer-friendly Version

Interactive Discussion

**Table 4.** Correlation coefficients between the integrated total particle number concentration from the SMPS with BC, NO<sub>x</sub>, and CO during each period for the two sites.

	Site	Period 1	Period 2	Period 3	Period 4
Correlation with BC	WHI	0.10	−0.57	0.71	0.89
	WRN	0.62	0.54	0.57	0.86
Correlation with NO <sub>x</sub>	WHI	0.21	−0.51	0.34	0.43
	WRN	0.49	0.26	0.09	0.59
Correlation with CO	WHI	−0.09	−0.13	−0.03	0.43
	WRN	0.49	−0.03	0.10	0.50
Correlation with SO <sub>2</sub>	WHI	0.45	−0.16	0.08	0.21
	WRN	−0.02	0.61	0.27	0.20

**Temperature-dependent accumulation mode particle**

L. Ahlm et al.

**Table 5.** Correlation coefficients between the biogenic PMF factor and CCN number of concentration at Raven's Nest for different supersaturations ( $S$ ).

	$r$ -coefficient
$S = 0.1$	0.35
$S = 0.2$	0.69
$S = 0.3$	0.78
$S = 0.5$	0.76

[Title Page](#)[Abstract](#)[Introduction](#)[Conclusions](#)[References](#)[Tables](#)[Figures](#)[⏪](#)[⏩](#)[◀](#)[▶](#)[Back](#)[Close](#)[Full Screen / Esc](#)[Printer-friendly Version](#)[Interactive Discussion](#)

**Temperature-dependent accumulation mode particle**

L. Ahlm et al.

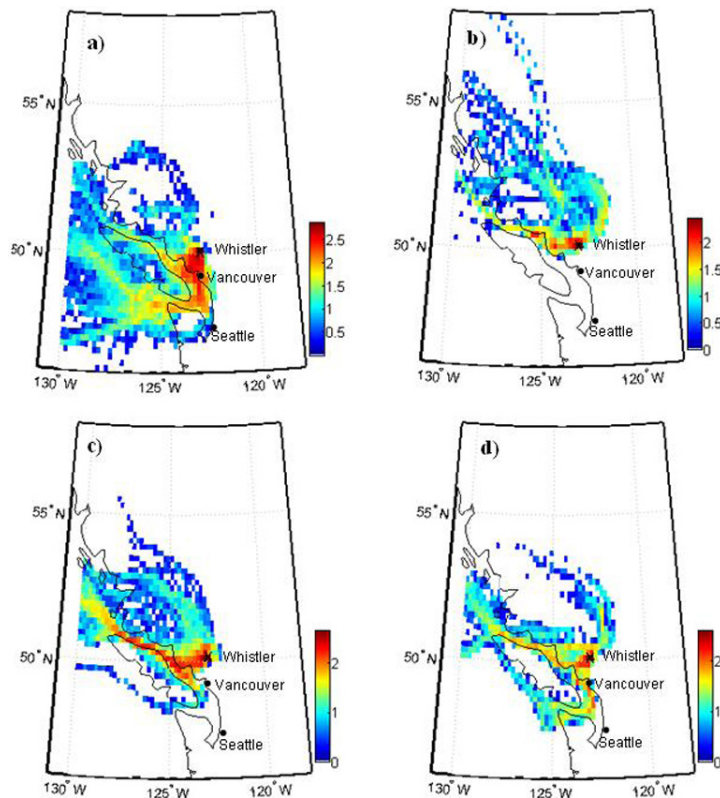


**Fig. 1.** HYSPLIT back trajectory (72 h) analysis for trajectories initiated at Whistler, with meteorological data sets from the Eta Data Assimilation System (EDAS) for **(a)** period 1, **(b)** period 2, **(c)** period 3, and **(d)** period 4. The color scale indicates  $\log_{10}$  of the number of trajectories that have passed through a certain grid cell. The grid cells are 0.2 degrees wide in both latitudinal and longitudinal direction. For every day 24 back trajectories have been calculated with an interval of one hour between each trajectory.

[Title Page](#)[Abstract](#)[Introduction](#)[Conclusions](#)[References](#)[Tables](#)[Figures](#)[⏪](#)[⏩](#)[◀](#)[▶](#)[Back](#)[Close](#)[Full Screen / Esc](#)[Printer-friendly Version](#)[Interactive Discussion](#)

## Temperature-dependent accumulation mode particle

L. Ahlm et al.

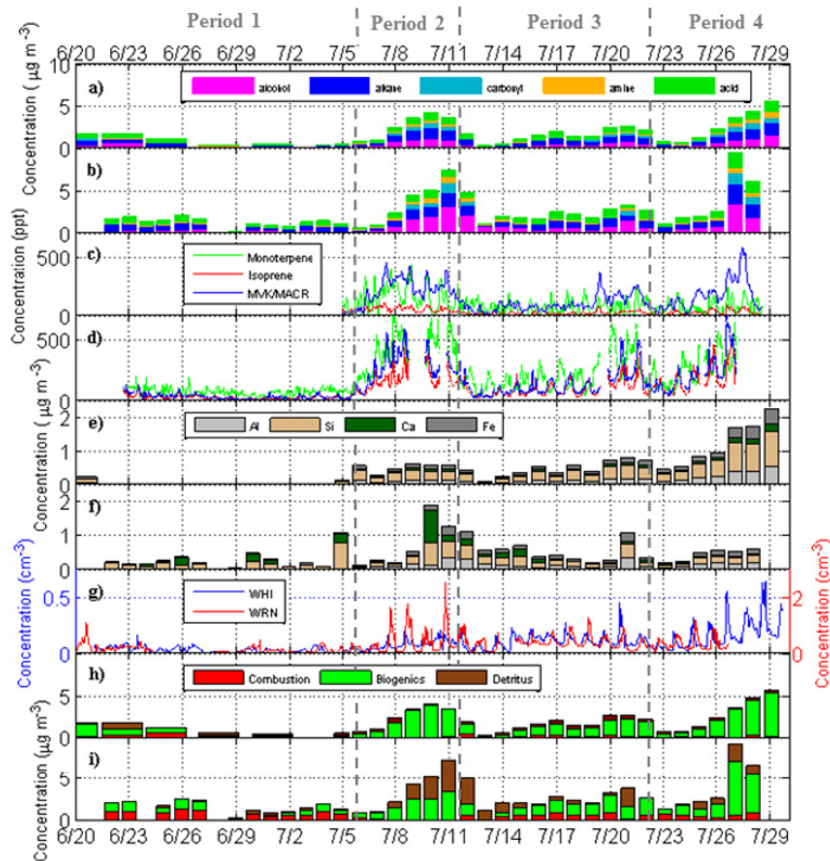


**Fig. 2.** Time series of FTIR organic functional groups at WHI (a) and WRN (b), PTR-MS VOCs at WHI (c) and WRN (d), XRF dust elements at WHI (e) and WRN (f), coarse particle number concentrations (g), and PMF factors at WHI (h) and WRN (i).

[Title Page](#)
[Abstract](#)
[Introduction](#)
[Conclusions](#)
[References](#)
[Tables](#)
[Figures](#)
[◀](#)
[▶](#)
[◀](#)
[▶](#)
[Back](#)
[Close](#)
[Full Screen / Esc](#)
[Printer-friendly Version](#)
[Interactive Discussion](#)

## Temperature-dependent accumulation mode particle

L. Ahlm et al.

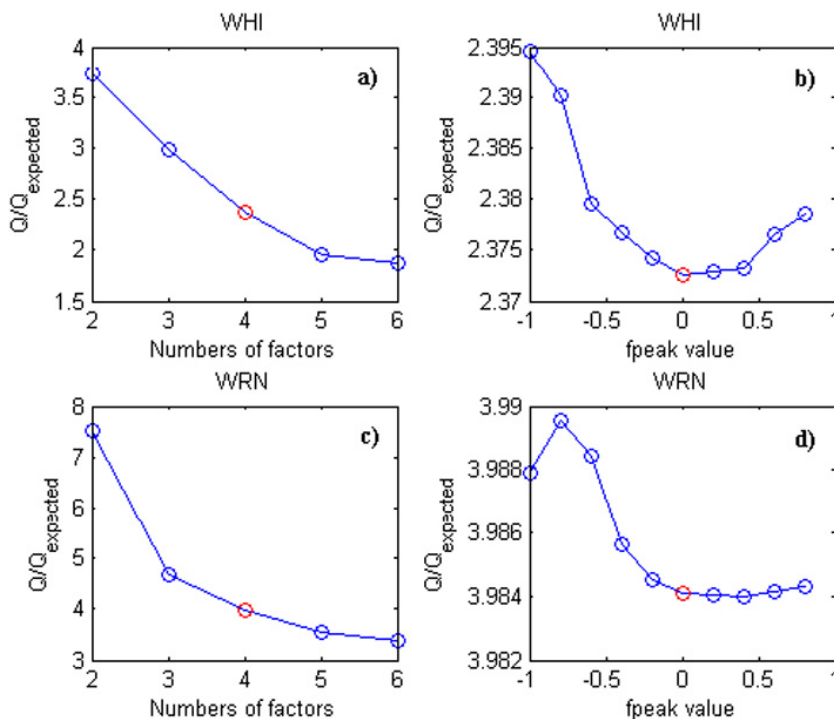


**Fig. 3.**  $Q/Q_{\text{expected}}$  for Whistler Peak against (a) numbers of factors used, and (b)  $f_{\text{peak}}$  values for 4 factors.  $Q/Q_{\text{expected}}$  for Raven's Nest against (c) numbers of factors used, and (d)  $f_{\text{peak}}$  values for 4 factors. The red circles show the chosen factor solution.

[Title Page](#)
[Abstract](#)
[Introduction](#)
[Conclusions](#)
[References](#)
[Tables](#)
[Figures](#)
[◀](#)
[▶](#)
[◀](#)
[▶](#)
[Back](#)
[Close](#)
[Full Screen / Esc](#)
[Printer-friendly Version](#)
[Interactive Discussion](#)

## Temperature-dependent accumulation mode particle

L. Ahlm et al.

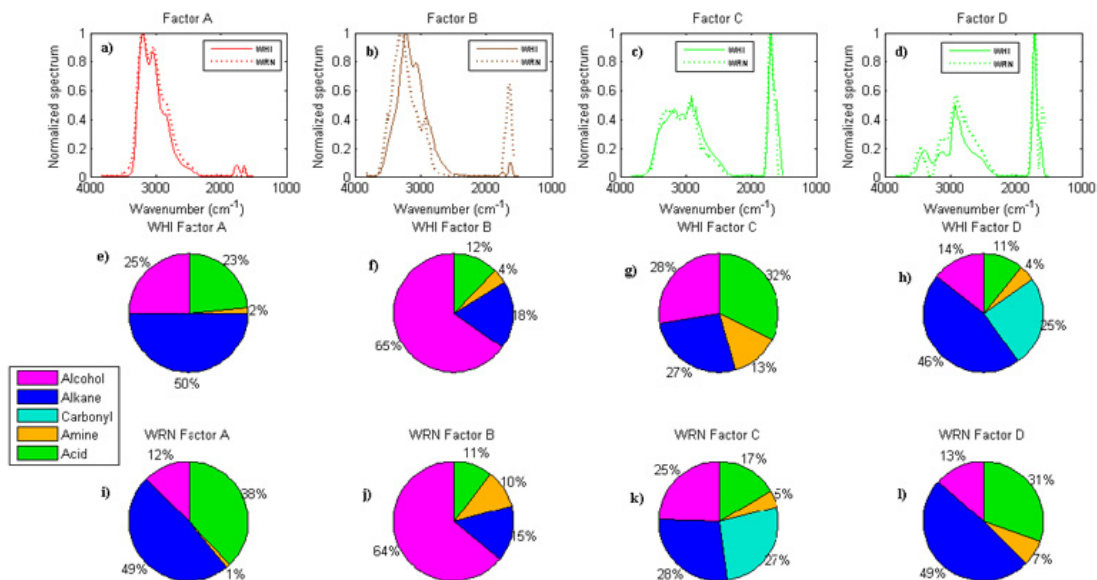


**Fig. 4.** PMF factor spectra for factors A–D for WHI (solid lines) and WRN (dotted lines) (a–d). Contributions from the different organic functional groups to factors 1–4 at WHI (e–h) and WRN (i–l).

Title Page

Abstract

Introduction

Conclusions

References

Tables

Figures

◀

▶

◀

▶

Back

Close

Full Screen / Esc

Printer-friendly Version

Interactive Discussion

## Temperature-dependent accumulation mode particle

L. Ahlm et al.

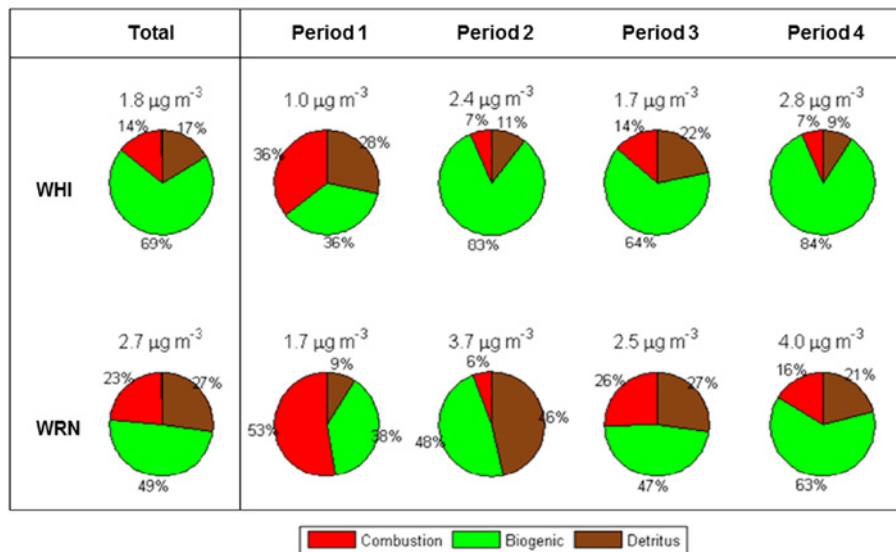


**Fig. 5.** Contributions from each PMF factor to the organic aerosol mass at WHI and WRN for the whole campaign, and for the four sub-periods. The indicated concentration above each pie chart represents the average organic concentration for the specific period and site.

[Title Page](#)
[Abstract](#)
[Introduction](#)
[Conclusions](#)
[References](#)
[Tables](#)
[Figures](#)




[Back](#)
[Close](#)
[Full Screen / Esc](#)
[Printer-friendly Version](#)
[Interactive Discussion](#)

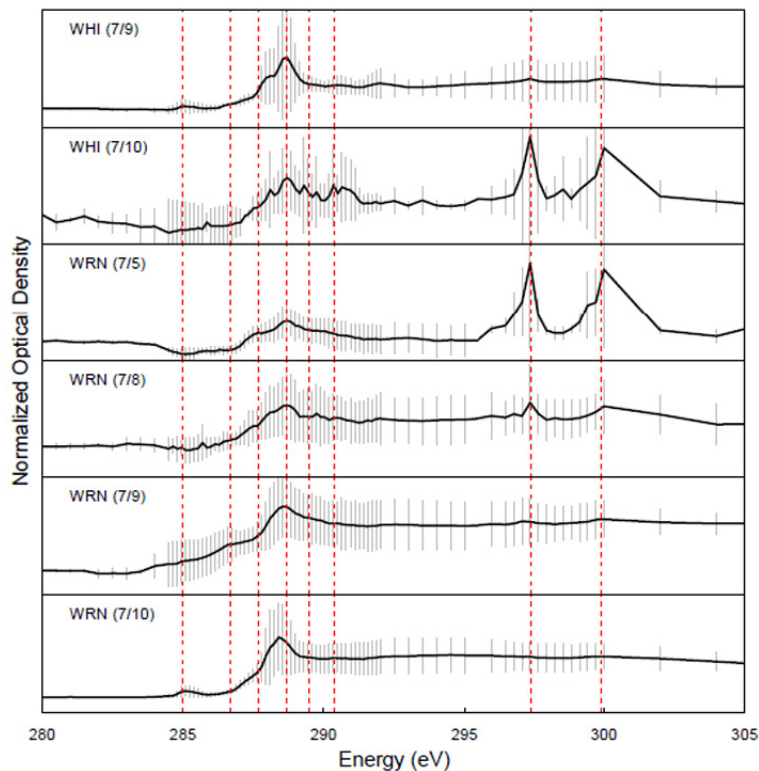


**Fig. 6.** The black solid lines represent the average of spectra of the particles from a specific sample. Grey vertical lines represent the standard deviation. Red dotted lines show the locations of the functional groups: 285 eV for alkene, 286.7 eV for ketonic carbonyl, 287.7 eV for alkyl, 288.7 eV for carboxylic carbonyl, 289.5 eV for alcohol, 290.4 eV for carbonate, and 297.4 and 299.9 eV for *K* absorptions.

**Temperature-dependent accumulation mode particle**

L. Ahlm et al.

Title Page

Abstract Introduction

Conclusions References

Tables Figures

⏪ ⏩

◀ ▶

Back Close

Full Screen / Esc

Printer-friendly Version

Interactive Discussion



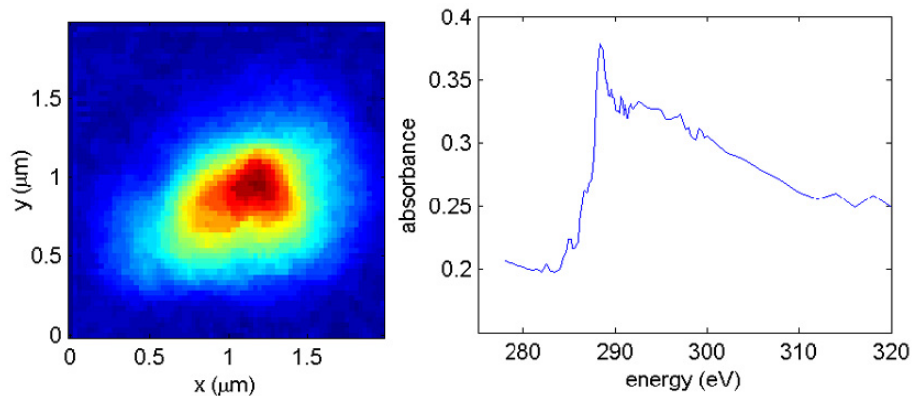


**Fig. 7.** An example of a particle with strong absorption in the COOH region (288.7 eV). The left plot shows the representative absorbance image at 288.85 eV, and the right plot shows the average absorbance spectrum.

**Temperature-dependent accumulation mode particle**

L. Ahlm et al.

Title Page

Abstract Introduction

Conclusions References

Tables Figures

⏪ ⏩

◀ ▶

Back Close

Full Screen / Esc

Printer-friendly Version

Interactive Discussion



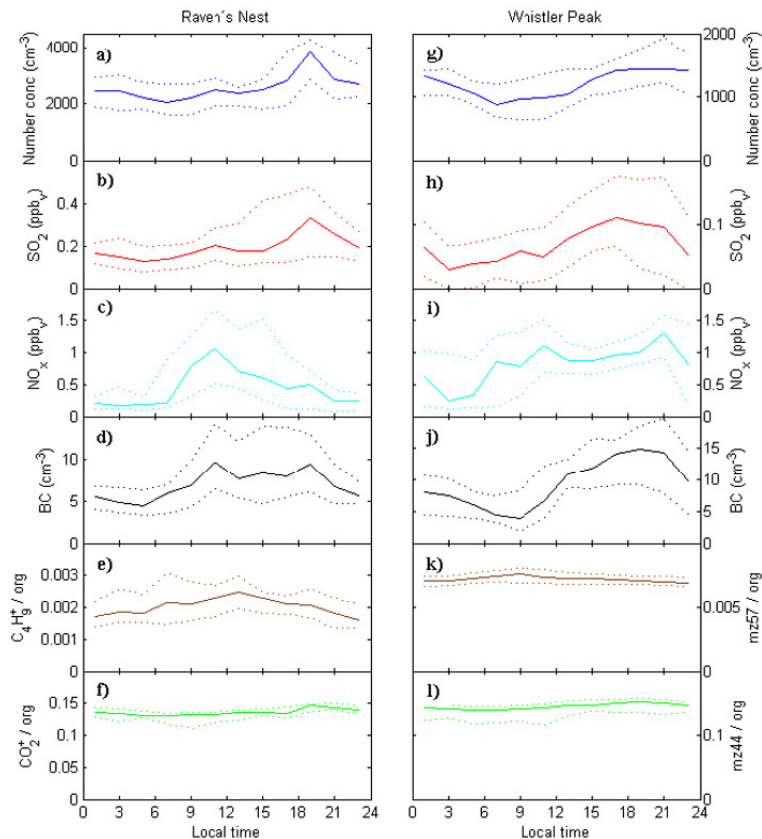


**Fig. 8.** Median diurnal cycles 13–22 July of total integrated SMPS particle number concentration,  $\text{SO}_2$ ,  $\text{NO}_x$ , and BC at Raven's Nest (a–d), and Whistler Peak (g–j). The ratios of  $\text{C}_4\text{H}_9^+$  and  $\text{CO}_2^+$  to total organic concentration at Raven's Nest (e–f), and the ratios of  $m/z$  57 and  $m/z$  44 to total organic concentration at Whistler Peak (k–l). Dotted lines represent 25 and 75 percentiles, respectively.

## Temperature-dependent accumulation mode particle

L. Ahlm et al.

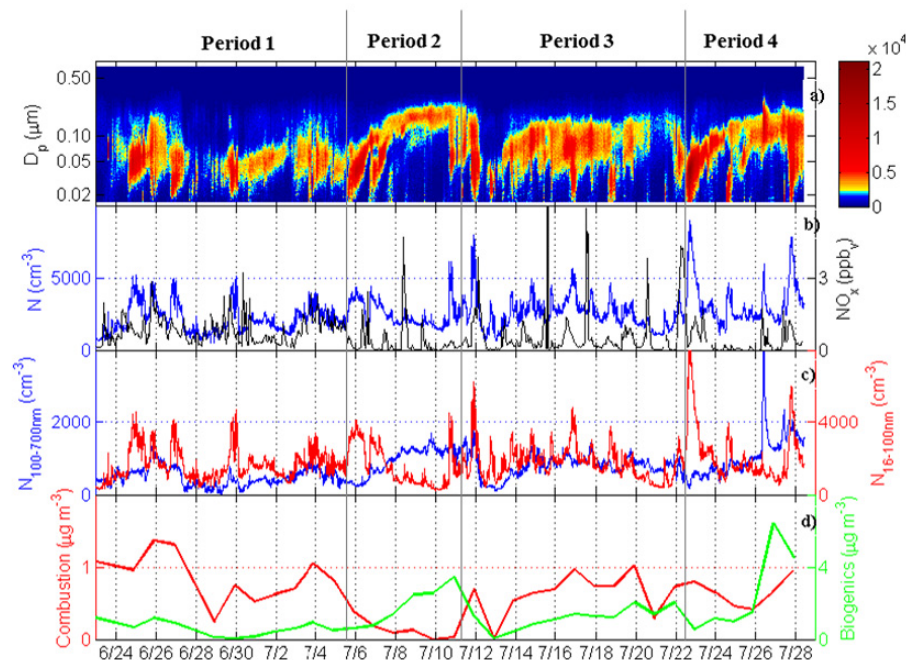


**Fig. 9.** Time series at Raven's Nest of **(a)** SMPS particle number size distribution (the color indicates  $dN/d\log_{10} D_p$  [ $\text{cm}^{-3}$ ]), **(b)** SMPS total integrated particle number concentration (blue) and  $\text{NO}_x$  concentration (black), and **(c)**  $N_{100}$  (blue) and  $N_{16-100}$  (red), and **(d)** the PMF combustion factor (red) and biogenic factor (green).

[Title Page](#)
[Abstract](#)
[Introduction](#)
[Conclusions](#)
[References](#)
[Tables](#)
[Figures](#)
[◀](#)
[▶](#)
[◀](#)
[▶](#)
[Back](#)
[Close](#)
[Full Screen / Esc](#)
[Printer-friendly Version](#)
[Interactive Discussion](#)

## Temperature-dependent accumulation mode particle

L. Ahlm et al.

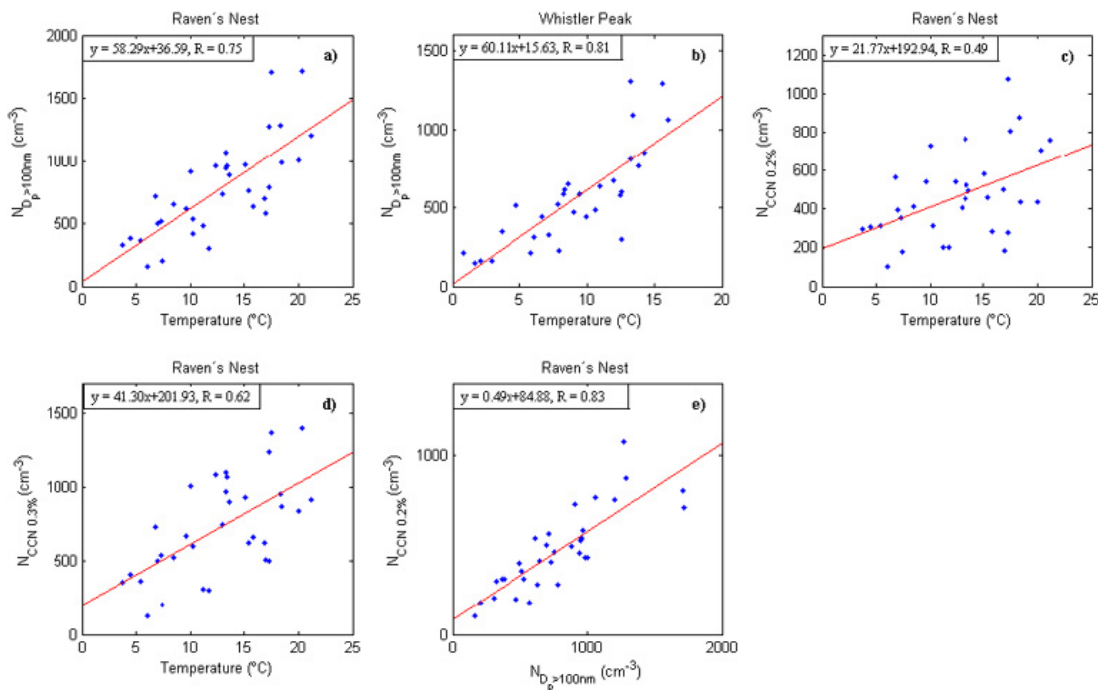


**Fig. 10.** Temperature dependency for numbers of particles with  $D_p > 100$  nm at Raven's Nest **(a)**, Whistler Peak **(b)**, for numbers of CCN at Raven's Nest at a supersaturation of 0.2% **(c)**, 0.3% **(d)**, and the relation between concentrations of CCN at a supersaturation of 0.2% and particles with  $D_p > 100$  nm at Raven's Nest **(e)**. Each point represents a 24 h average. The red curves represent linear fits according to the given equation in each plot.

Title Page

Abstract

Introduction

Conclusions

References

Tables

Figures

◀

▶

◀

▶

Back

Close

Full Screen / Esc

Printer-friendly Version

Interactive Discussion